Review of open neuromorphic architectures and a first integration in the RISC-V PULP platform

Impact response of adhesive reversible joints made of thermoplastic nanomodified adhesive

Authors:
R. Ciardiello[a], A. Tridello[b], V. Brunella[c], B. Martorana[d], D.S. Paolino[e], G. Belingardi[f]

[a,b,e,f] Department of Mechanical and Aerospace Engineering, Politecnico di Torino, 10129 Turin, Italy,
[a]raffaele.ciardiello@polito.it, [b]andrea.tridello@polito.it, [e]davide.paolino@polito.it,
[f]giovanni.belingardi@polito.it
[c]Department of Chemistry and NIS Research Centre, University of Torino, 10125 Torino, Italy
valentina.brunella@unito.it
[d]Centro Ricerche Fiat S.C.p.A.,Group Materials Labs, 10135 Torino,Italy
brunetto.martorana@crf.it

Corresponding Author:
Raffaele Ciardiello
E-mail address: raffaele.ciardiello@polito.it
Full postal address:
C.so Duca degli Abruzzi 24,
Department of Mechanical and Aerospace Engineering – Politecnico di Torino,
10129 – Turin,
ITALY

Abstract

The impact response of a reversible adhesive joint is experimentally assessed in this work. Joint reversibility is improved with a system that uses nanomodification of the thermoplastic adhesive used for bonding plastic components. This system, coupled with electromagnetic induction, is able to guarantee separation of the joints without any damage to the substrates. Drop dart tests at different impact velocities are carried out on neat and nanomodified bonded joints in order to compare the impact behaviour before and after the introduction of nanoparticles. Experimental results show that the impact response, assessed in terms of peak load, absorbed energy and flexural stiffness, can be affected by the introduction of nanoparticles. This work shows that adhesive nanomodified joints represent an effective and applicable solution for the reversible assembling of semi-structural components subjected to low-velocity impact loads.

Keywords: Hot-melt, impact, nanomaterials, automotive, polyolefins.

1. Introduction

In the last decades, the use of adhesives in many machinery applications has rapidly increased. Adhesive joints are often preferred to traditional mechanically fastened joints due to the advantages that they offer. If well designed [1,2], adhesive joints exhibit a better stress distribution compared to the traditional fasteners and high mechanical properties under different loading conditions [3,4]. Adhesives could also have a higher resistance to environmental factors [5] and they are usually preferred to traditional fasteners when joining components made of different materials [6,7].

A wide variety of adhesives is currently available and structural and non-structural adhesives are largely adopted. Thermoset adhesives are generally employed for structural joints but recently there has also been a significant increment in the use of thermoplastic adhesives. In some specific applications, thermoplastic adhesives are even preferable to traditional thermoset adhesives due to their ease of application and their flexibility in joining different kinds of plastic materials that are sometimes hard to bond, such as polypropylene (PP) [8]. Indeed, the diffusion of PP based materials is increasing in many industrial fields, especially in the automotive field [9], and this is a further reason for the increment in the use of thermoplastic adhesives.

In the automotive field, thermoplastic polyolefinic hot-melt adhesives (HMAs) are commonly adopted to assemble interior and exterior parts. For example, this kind of adhesives is largely used to bond plastic bumper fascia to a structural plastic support [10]. Since plastic bumper fascia is mainly subjected to impact loading and, in particular, to low-velocity impacts in the range 2-27 km/h [11-13], the adhesive and the related joint are frequently subjected to low-velocity impacts as well. Typical examples of low-velocity impacts are represented by front to rear vehicle impacts and debris impacts. After the impact event, plastic bumpers often need to be disassembled from the plastic support for maintenance operations, which could be significantly simplified if the adhesive joint can be easily separated. Therefore, simplification of the disassembly procedure is a major point of interest for the automotive industry.

HMAs can be separated by heating the adhesive until the melting temperature is reached [14]. However, the melting temperature of the HMA is close to the melting temperature of the plastic substrates, and the disassembly process can introduce severe damage to these substrates. In order to set a viable solution for the disassembly procedure, innovative joining techniques have been recently proposed in the literature [15-20]. Among these, HMAs embedded with magnetic nanoparticles represent an effective solution. They can even enhance the mechanical properties of the adhesive and, consequently, of the assembled part. According to [21-24], the nanomodification has a positive effect on the mechanical properties of the materials, especially on their impact response. In [21], it is shown

that ceramic nanoparticles can significantly enhance (from 4% to 15% of increment of absorbed energy) the impact response in a speed range between 2 m/s and 8 m/s. Avila et al. [22] showed that epoxy resin modified with nanoclay has greater stiffness and can absorb larger energy rate during impact. The same nanofiller with the same weight percentage was used by Avila et al. in [23] as skins of sandwich structure. Their study shows that the addition of 5% of nanoclay leads to an increase of energy absorption. Xie et al. [24] showed that polyvinyl chloride (PVC) modified with nanosized antimony trioxide particles with different weight concentrations (2.5%, 5% and 7.5%) can increase the energies needed for crack initiation and propagation. Therefore, literature results show that nanomodification positively affects the impact response of materials. However, to the authors' best knowledge, no experimental result is available in the literature on the impact response of nanomodified HMAs. Since HMA joints currently employed in the automotive industry are mainly subjected to low-velocity impacts and they frequently need to be disassembled, the experimental characterization of the impact response of nanomodified HMAs is of utmost interest.

In this work, the effect of nanomodification on the impact response of polypropylene beams bonded with a thermoplastic HMA is experimentally assessed. Drop dart tests at different impact velocities are carried out on neat and nanomodified joints. Single and repeated impact tests are performed in order to compare the impact response in terms of peak load, adsorbed energy and flexural stiffness with and without nanomodification.

2. Materials and methods

In this Section, the investigated materials and the experimental activities are illustrated in detail. Section 2.1 describes the materials and the procedure adopted for the preparation of the adhesive joints. In Section 2.2, the experimental setup and the methodology used for the analysis of the experimental data are explained in detail.

2.1 Materials

The joints used for the experimental tests were obtained by bonding adherents made of a polypropylene copolymer with 10% in weight of talc, (Hifax CB 1160 G1, by Lyondell-Basell Industries, Houston, United States). Rectangular beams, 100 mm long with cross-section 20×3 mm, were used for the experimental tests.

The beams were bonded with Prodas, a polyolefin-based HMA by Beardow Adams (Milton Keynes, United Kingdom), a copolymer of polypropylene and polyethylene [18]. The nanomodified adhesive was prepared using a hot plate for melting the neat adhesive and by adding 10% in weight of iron oxide particles with size smaller than 50 nm (Fe_3O_4 by Sigma-Aldrich, Saint Louis, United States). Following a procedure commonly adopted in the literature for HMAs [8,11,13,15], pellets were melted together at 190°C, using the hot plate. At 190°C, the viscosity of the adhesive is low enough to easily mix the particles into the adhesive by mean of a glass rod. The iron oxide nanoparticles were added gradually and mixed together with the adhesive.

Joint preparation was performed with a hot-melt gun (Figure 1a) and an assembly device (Figure 1b) which make it possible to control the thickness of the adhesive joint.

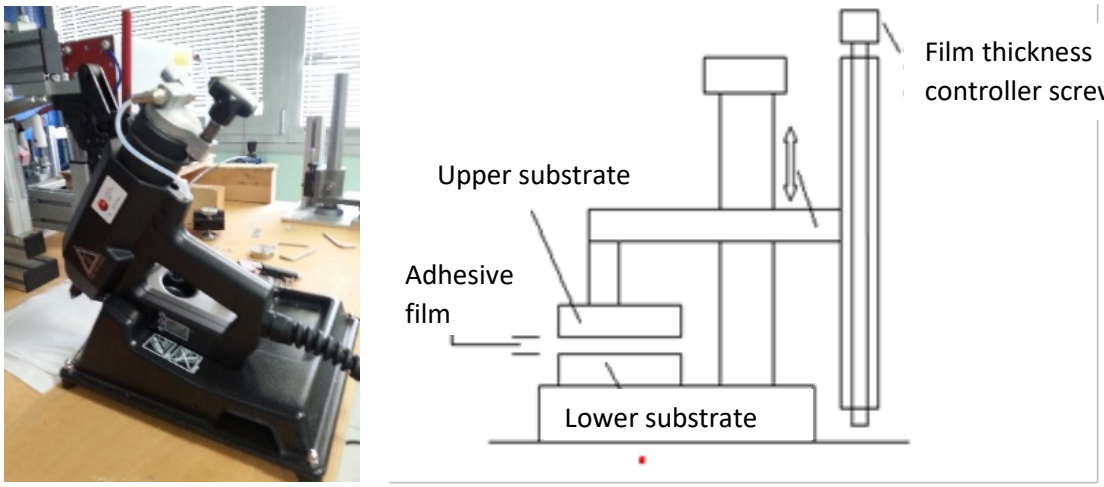

a) b)

Figure 1: Instrumentation used for the joint preparation: a) hot melt gun; b) assembly device [18].

Nominal thickness of the adhesive layer is $1\ \mathrm{mm}$. As shown in Figure 1b, a film-thickness controller screw was used to fix the thickness of the adhesive layer at the desired value. Firstly, the adherent (lower substrate in Figure 1b) was fixed on the lower base of the assembly device. Then, the HMA at high temperature was uniformly spread over the lower substrate by means of the hot melt gun. An amount of adhesive larger than necessary was used to ensure that the overlap of the lower substrate was completely covered. Then, the upper adherent (upper substrate in Figure 1b) was placed on the still melted adhesive. A weight of $(3.5\ \mathrm{kg})$ was placed on the support of the upper adherent, in order to eliminate the excess adhesive. The procedure squeezed out the excess adhesive until the required adhesive thickness was reached.

The thickness of each joint was measured and was found to be constant along the joint length, with a variation smaller than $0.05\ \mathrm{mm}$. When the adhesive was solidified, the adhesive in excess was removed mechanically by means of a cutter.

Figure 2 shows a bonded joint used for the experimental tests. The nominal dimensions of the joint are also reported. All the reported dimensions are in millimetres.

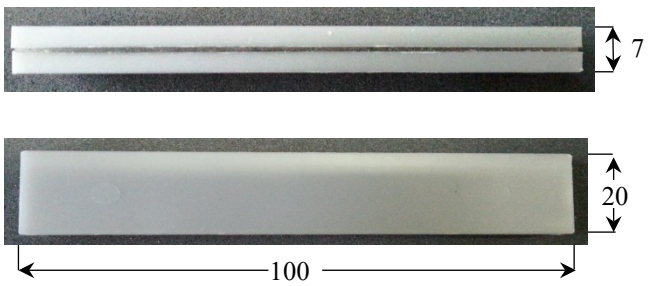

Figure 2: Bonded joint used for the experimental tests. Dimensions in mm.

Before the experimental tests, the dispersion of the iron oxide within the plastic matrix was verified using a Scanning Electron Microscope (SEM). SEM analyses were carried out using a Carl-Zeiss EVO50. The electronic high tension used was 20 kV and the secondary electron emission was used as signal. The specimens were coated with gold in order to have better images. The sample for the SEM observation was obtained by gradually heating a bonded joint at 80 °C, quite below the softening point of the HMA, and thereafter by easily separating the joint through a sharp cutter. The SEM analyses

were conducted on the smoothest area found through visual inspection. Two specimens were used for the SEM analysis.

Figure 3 shows a representative SEM image at 500X magnification of the nanomodified adhesive. The largest white shining spot in Figure 3 are due to the presence of some deposed residuals attached on the adhesive surface before the SEM analysis.

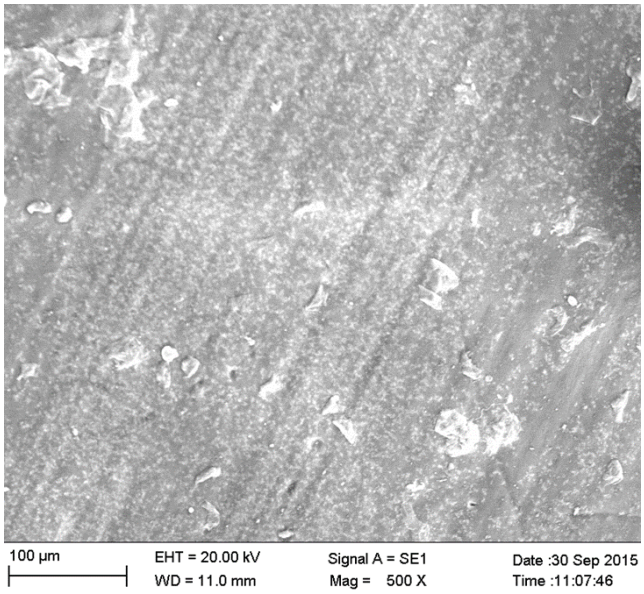

Figure 3: Representatitve SEM image at 500X of the nanomodified adhesive.

According to Figure 3, the tiny white spots are the iron oxide nanoparticles embedded in the HMA matrix. The distribution of these fillers within the adhesive is almost uniform: the total area without particles, evaluated through digital image processing, is equal to 854.1 μm^2 and it represents the 0.15% of the investigated area.

Figure 4a and 4b show SEM images of the modified adhesive at 5000x and at 10000x, respectively.

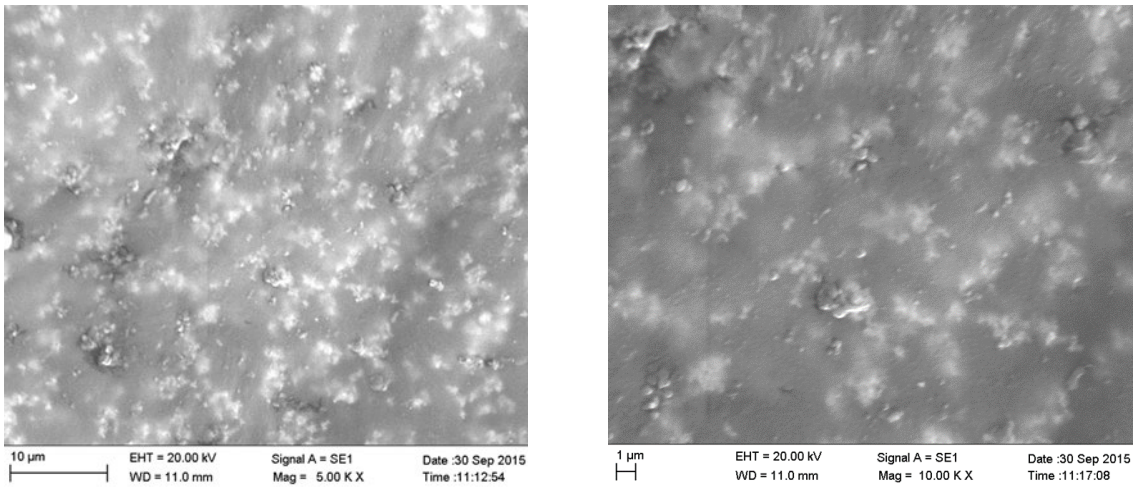

a) b)

Figure 4: SEM images of the nanomodified adhesive: a) 5000x image; b) 10000x image.

As can be seen in these figures, nanoparticles tend to form small aggregates. The aggregates dimension was assessed at fifteen different locations in Figure 4a. In particular, the average particle size was found to be equal to 0.86 µm, with a standard deviation 0.41 µm. The presence of these small aggregates is attributed to the nature of the particles that, before mixing, display a tendency to agglomerate as shown in Figure 5. Figure 5 shows the Atomic Force Microscope (AFM) analysis of the

particles used in this work. The AFM (Veeco Digital Instrument, Santa Barbara, USA) was used in tapping mode and with a Si_3N_4 cantilever. Figure 5 evidences that the dimension of a single particle is lower than 55 nm but particles aggregate as clusters with size very close to the one measured in the adhesive matrix. The lowest cluster length is around 0.78 µm.

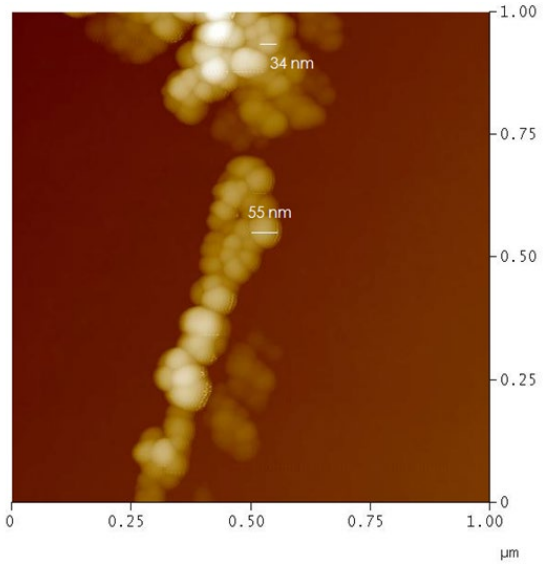

Figure 5: AFM of the iron oxide nanoparticles [16].

2.2 Flexural elastic modulus

Flexural elastic modulus of neat and nanomodified joint is assessed through the Impulse Excitation Technique (IET). According to the ASTM standard [25], the bonded joint is supported at the two nodal points of the first modal shape for driving the flexural mode of vibration. Through a small hammer with a spherical head (4 mm diameter), the joint is hit in the centre of the bar in order to excite the bending mode of vibration. A microphone is used to acquire the vibration amplitude at the free edge of the joint. The signal coming from the microphone is acquired by using a Data Acquisition Card (DAQ) and is used to assess the frequency response through the application of the Fast Fourier Transform algorithm. The flexural modulus is finally obtained according to [25]. Figure 6 shows the IET system used for the assessment of the flexural elastic modulus.

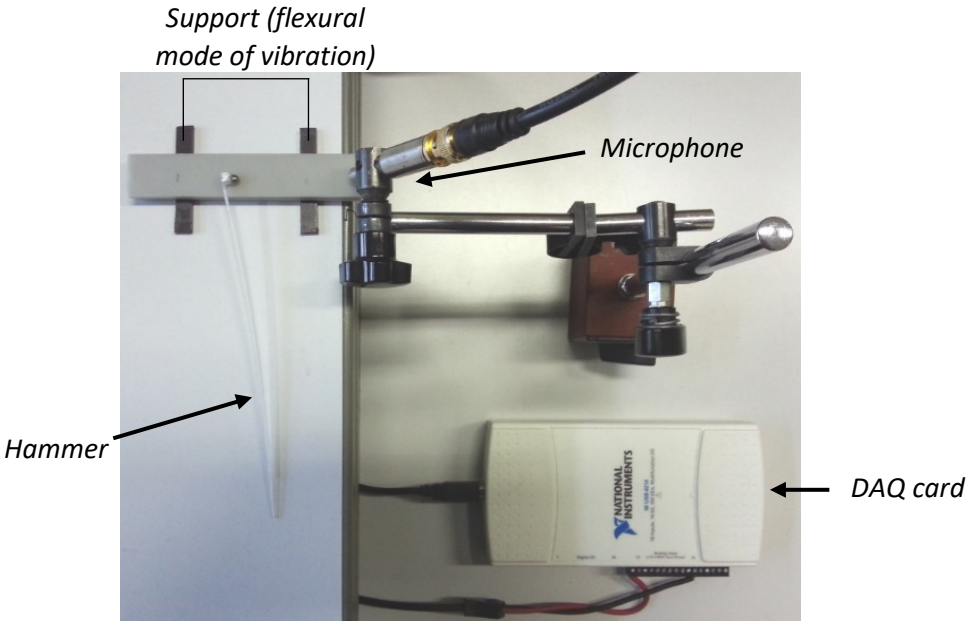

Figure 6: IET system for assessing the flexural elastic modulus.

IET tests wer carried out on two neat and two nanomodified joints. Three measurements for each joint wer performed. Figure 7 shows representative frequency spectra obtained with the IET tests on the neat (Figure 7a) and on the nanomodified joints (Figure 7b). The small boxes inside each figure show a magnification of the peak region.

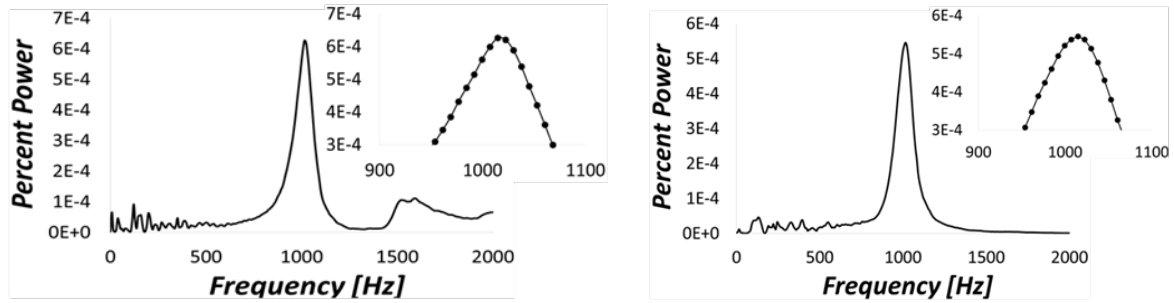

a) b)

Figure 7: IET spectra for the investigated joints: a) neat joint; b) nanomodified joint.

A negligible scatter, smaller than 7 Hz, is found in the spectra obtained experimentally. The flexural modulus is found to be in the range 1.9-2.0 GPa for the neat joint and in the range 1.9-2.1 GPa for the nanomodified joint. Therefore, the nanomodification does not significantly affect the flexural elastic modulus.

2.3 Impact test setup

Impact tests were carried out using a free-fall drop dart testing machine (CEAST 9350 FRACTOVIS PLUS) equipped with a 12.7 mm hemispherical impactor tup, for the assessment of the impact response. The different impact speeds were obtained by varying the drop height. For each impact test, the impact speed was measured using a magnetic encoder. The encoder measured the speed of the impactor just before it comes into contact with the specimen. Therefore, for each test, the actual speed before the impact was measured in order to accurately compute the impact energy. The speed signal was also used as a trigger to start the acquisition of the load signal, in order to reduce the amount of acquired

data. The joints to be tested were clamped at both ends by a mechanical clamping system which ensures a uniform pressure all over the clamping area, as shown in Figure 8.

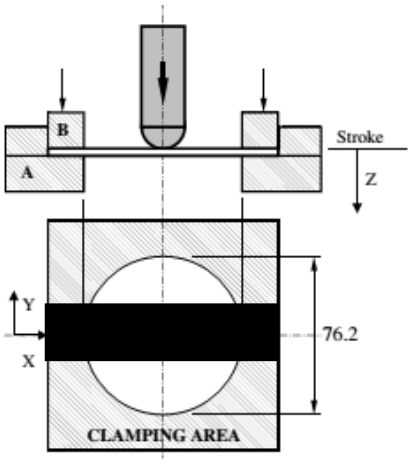

Figure 8: Clamping system for the impact tests. In black, the clamped specimen.

Load signal was acquired by using a piezoelectric load cell (203B by PCB Piezotronics, Depew, United States) with a sample rate of 1 MHz. According to [26,27] and by considering the energy balance equation during the impact, displacement-time curve was obtained by integrating twice the acquired load signal with respect to time. The adsorbed energy was finally obtained through an additional integration of the load with respect to the displacement.

Initial experimental plan envisaged to use two different velocities: 10 m/s, which gave, without any additional mass, an energy of 368 J, and 5 m/s with the same energy, through additional masses. Tests performed at 5 m/s gave repeatable results as can be seen in Figure 9. On the other hand, tests performed at 10 m/s did not give acceptable results, due to the slippage of specimens in the clamping fixture. Figure 9 shows the trend of the test performed at 10 m/s, together with the tests run at 5 m/s. The 10 m/s test exhibits a significant decrement of the force signal, in the displacement range from 5 mm (beginning of slippage) to 31 mm (end of the test). After the 10 m/s test, specimen was bent but not perforated. For these reasons, a lower velocity, equal to 8 m/s, was chosen for the subsequent tests. Tests at 8 m/s still permitted to evaluate the effect of the velocity in the limited range from 5 m/s to 8 m/s. Tests at 8 m/s gave repeatable results, as can be seen in Figure 11 in the next section.

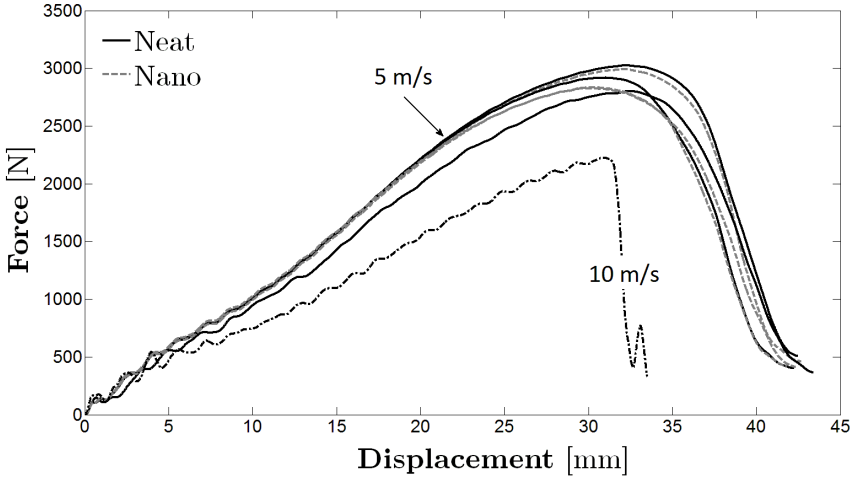

Figure 9: Force-displacement curves at 5 m/s and 10 m/s.

The behaviour of the joint was also investigated in a different damage condition, with repeated impacts at low energy that did not lead to perforation even for a high number of impacts. From the perforation tests, it was possible to evaluate the maximum perforation energy of the joint. Ten impacts with an energy of 8 J (around 10% of the value of the perforation energy) are then carried out in order to assess the behaviour of the joint under repeated impacts. The chosen impact energy guarantees a low damage accumulation impact after impact, according to [28].

Perforation impact tests on neat and nanomodified joints were performed at an impact speed of $5\ \mathrm{m/s}$. The effect of velocity was investigated by testing the joints at a higher speed of 8 m/s with the same impact energy.

Repeated impact response was also experimentally evaluated. To this aim, ten repeated impact tests at low energy (8 J) are performed. Residual elastic modulus after the last impact was evaluated through the IET. The experimental activity is summarized in Table 1.

Table 1: summary of the experimental impact activity

	Impact velocity [m/s]	*Impact energy [J]*	*Number of repetitions*	*Impact mass [kg]*
Perforation tests	5	368	3	29.4
	8	368	3	11.5
Repeated impacts (10 impacts)	1.5	8	2	7.4

3. Experimental results: Perforation tests

Perforation tests were carried out at an impact energy significantly larger than the estimated perforation energy of the specimen.

During each perforation test, bars were split into two parts of almost equal length. An example of a joint after the perforation impact can be seen in Figure 10. Failure modes of neat and nanomodified joints are found to be very similar and no difference is found between failure modes in impact tests performed at different velocities.

Figure 10: An example of a neat joint after perforation.

Experimental data were analyzed with a script written in Matlab®. Figure 11 shows the force-displacement and the energy-displacement curves for the neat and nanomodified joints tested at $5\ \mathrm{m/s}$ (Figures 11a and 10c) and $8\ \mathrm{m/s}$ (Figures 11b and 10d).

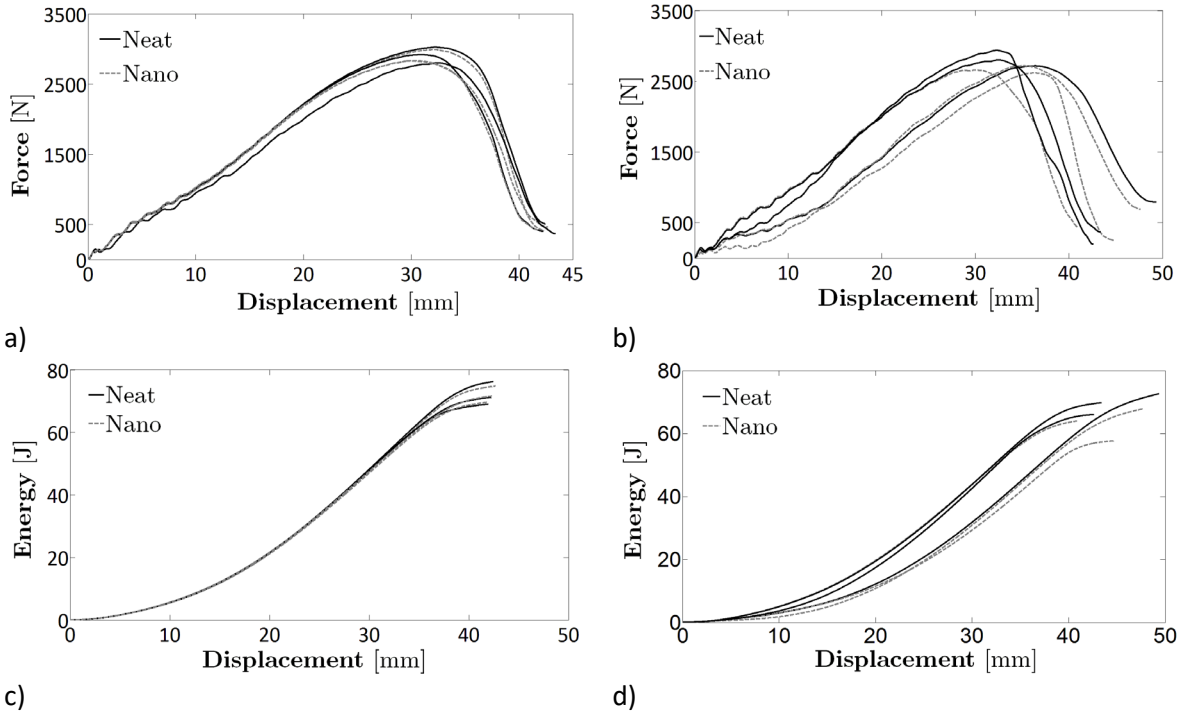

Figure 11: Perforation curves: a) Force-displacement at $5\ \mathrm{m/s}$; b) Force-displacement at $8\ \mathrm{m/s}$; c) Energy-displacement at $5\ \mathrm{m/s}$; d) Energy-displacement at $8\ \mathrm{m/s}$.

Figure 11 evidences that the impact responses of neat and nanomodified joints are quite similar: curves follow same qualitative trends. Repeatability is good and curves are concentrated within a limited region.

Table 2 summarizes the experimental results obtained after the perforation impact tests on the neat and nanomodified bonded joints. Maximum and minimum values of peak force, absorbed energy and stiffness are reported in Table 2. According to [26], flexural stiffness is evaluated as the slope of the initial straight line in the force-displacement curve.

Table 2: Experimental dataset for the perforation impact tests.

	Impact velocity [m/s]	*Peak force [N]*	*Energy [J]*	*Stiffness [N/mm]*
Neat	5	[2907;3024]	[69;76]	[107.4;107.7]
	8	[2717;2917]	[66;74]	[99; 112]
Nanomodified	5	[2881;3023]	[69;74]	[103;107]
	8	[2787; 2832]	[59; 69]	[101;107]

As can be seen in Figure 11 and Table 2, the experimental results for the nanomodified adhesive show a larger scatter. The introduction of nanoparticles can locally modify the mechanical properties of the adhesive and it can affect the experimental response (SEM analysis in Section 2.1).

A statistical analysis was therefore carried out in order to evaluate if the nanomodification significantly influenced the impact response of the investigated thermoplastic bonded joint. The effect of velocity was also investigated both for the neat and the nanomodified bonded joint. Analysis of Variance

(ANOVA) was used to statistically compare the data. In the following section, the ANOVA analysis is applied to peak force, absorbed energy and stiffness. Two factors were investigated (i.e., nanoparticles N and velocity V), with three replications for each treatment combination. A 90% and a 95% confidence level was considered in the analysis.

The resulting ANOVAs are reported in Sections 3.1 to 3.3. The main parameters used in the calculation of the ANOVA are reported in each table: Sum of Squares (SS), Degrees of Freedom (DOF), Mean Squares (MS) and Fisher ratios (F) were computed from the experimental data. F95% and F90% are the 95% and 90% percentiles of the Fisher distribution. The ratio between the experimental SS (sum of squared deviations from a mean value) and the DOF (number of factor levels minus 1) permits the determination of MS (i.e., MS = SS / DOF). The computed MS is used to assess the significance of each factor (factor N and V) and interaction between factors (Interaction N-V). The significance analysis was performed for each factor and interaction through the statistical hypothesis test proposed by Fisher (F-test). For each factor and interaction, the statistics F (ratio between the MS related to each factor, MS_N and MS_V, and interaction, MS_{N-V}, and the MS related to the Error, MS_E) is compared with the considered percentile of the Fisher distribution. If F is larger than the percentile (i.e., F95% or F90% in the reported ANOVAs), then the corresponding factor or interaction significantly influences the investigated response (peak force, absorbed energy or stiffness), according to the confidence level (90% or 95%) assumed for the test.

3.1 Peak force

Table 3 reports the results of the ANOVA for the peak force.

Table 3: ANOVA for the peak force.

Source	***SS***	***DOF***	***MS***	***F***	***F95%***	***F90%***
Nanoparticles (N) *	30070	1	MS_N=30070	F_N=4.39	5.32	3.46
Velocity (V) **	40751	1	MS_V=40751	F_V=5.95	5.32	3.46
Interaction N-V	5071	1	MS_{N-V}=5071	F_{N-V}=0.74	5.32	3.46
Error	54811	8	MS_E=6851			
Total	130704	11				

Note: stars denote level of confidence: one star for 90% confidence level; two stars for 95% confidence level

As can be seen in the table, for the investigated range of velocities, velocity and the introduction of the nanoparticles affect the peak force when a 90% confidence level is considered. Velocity affects impact response also with a 95% confidence level. On the other hand, the interaction between velocity and the introduction of nanoparticles does not affect impact response for the peak force.

3.2 Absorbed energy

Table 4 reports the results of the ANOVA for the absorbed energy.

Table 4: ANOVA for the absorbed energy.

Source	*SS*	*DOF*	*MS*	*F*	*F95%*	*F90%*
Nanoparticles (N)	36.75	1	MS_N=36.75	F_N=2.20	5.32	3.46
Velocity (V) *	60.75	1	MS_V=60.75	F_V=3.64	5.32	3.46
Interaction N-V	24.08	1	MS_{N-V}=24.08	F_{N-V}=1.44	5.32	3.46
Error	133.33	8	MS_E=16.66			
Total	254.91	11				

Note: stars denote level of confidence: one star for 90% confidence level; two stars for 95% confidence level

Table 4 shows that nanoparticles do not affect the absorbed energy when a 90% and 95% confidence level is considered. On the other hand, velocity affects impact response when a 90% confidence level is considered. The interaction between the two parameters does not affect impact response for the adsorbed energy.

3.3 Stiffness

Table 5 reports the results of the ANOVA for the stiffness.

Table 5: ANOVA for the stiffness.

Source	*SS*	*DOF*	*MS*	*F*	*F95%*	*F90%*
Nanoparticles (N)	13.19	1	MS_N=13.19	F_N=0.81	5.32	3.46
Velocity (V)	21.05	1	MS_V=21.05	F_V=1.29	5.32	3.46
Interaction N-V	0.32	1	MS_{N-V}=0.31	F_{N-V}=0.02	5.32	3.46
Error	130.07	8	MS_E=16.25			
Total	164.64	11				

Note: stars denote level of confidence: one star for 90% confidence level; two stars for 95% confidence level

Finally, the ANOVA on the stiffness confirms that no statistical difference exists before and after the introduction of the nanoparticles and velocity does not affect impact response when both F95% and F90% are considered.

3.4 Repeated impacts

The experimental response to repeated impacts is analyzed in this Section. Experimental data are assessed according to the methodology described in Section 2.2. Figure 12 shows the normalized peak force (F_{max} normalized with respect to the peak force at the first impact, $F_{max,1}$) versus the impact number.

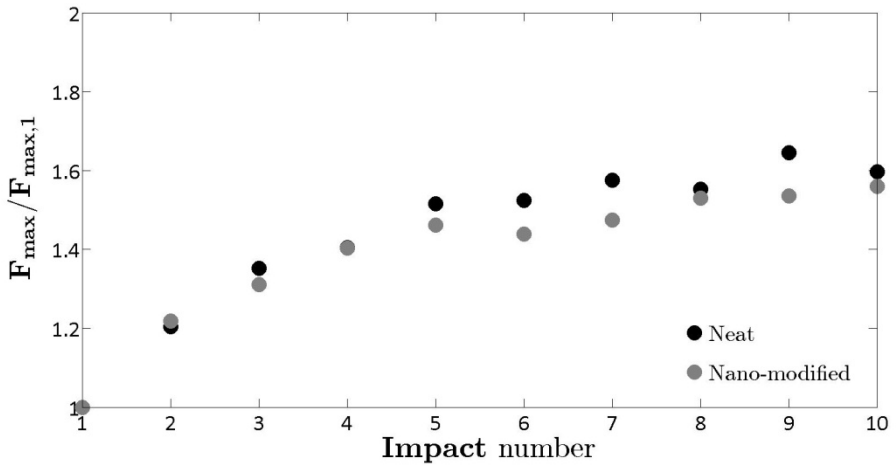

Figure 12: Normalized peak force with respect to the impact number.

Figure 12 evidences that the peak force trends are almost similar for the neat and nanomodified joints. In particular, the peak force tends to increase in the first five impacts, whereas it keeps constant after the sixth impact. The degradation of the elastic modulus after the repeated impact tests was experimentally assessed through the IET. IET was applied to the damaged neat and the nanomodified joints, with the same configuration described in Section 2.2. Figure 13 shows representative frequency spectra obtained with the IET tests on a damaged neat (Figure 13a) and on a nanomodified joint (Figure 13b).

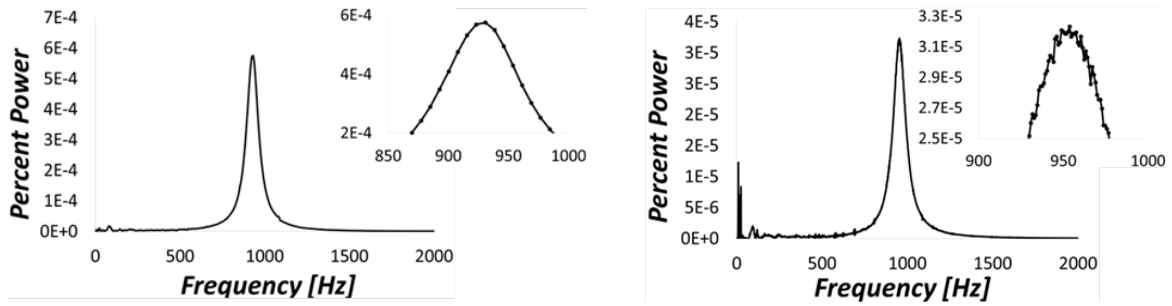

a) b)

Figure 13: IET spectra for the investigated damaged joints: (a) neat joint; (b) nanomodified joint.

As can be seen, the resonance peak decreases due to the damaged introduced by the repeated impacts. By contrast, in Figure 4, the resonance peak was about 1015 Hz for both joints, whereas, after ten repeated impact tests, the resonance peak decreased to about 950 Hz. For each damaged joint, three measurements were performed. The peak for the nanomodified joint shows a larger noise, probably due to a non-uniform distribution of the particles within the adhesive after the impact. However, the peak is clear and the larger noise does not affect the computation of the residual elastic modulus.

Table 6 compares the elastic modulus before and after the repeated impact tests. E_f is the flexural elastic modulus before the repeated impact tests. $E_{f,r}$ is the residual elastic modulus of the joint after the last impact. Minimum and maximum moduli are reported in the table.

Table 6: Flexural elastic modulus of the bonded joints before and after the repeated impact tests.

	E_f *[GPa]*	$E_{f,r}$ *[GPa]*
Neat	[1.9 ; 2.0]	[1.3 ; 1.4]
Nanomodified	[1.9 ; 2.1]	[1.4 ; 1.5]

As shown in Table 6, the decrement of the elastic modulus is equivalent for the neat and the nanomodified joint. After ten impacts, the average decrement is about 30%. Therefore, the introduction of the nanoparticles does not influence the repeated impact response of the investigated joint.

4. Conclusions

The objective of this work was to evaluate the impact response of a nanomodified thermoplastic adhesive, which is currently used in the automotive field for parts subjected to low-velocity impacts. Single and repeated impact tests were carried out on neat and nanomodified (with iron oxide) joints.

Experimental results and ANOVA show that the introduction of a 10% in weight of nanoparticles, using a 90% significance level, influences the impact response of the joint only for the peak force. Obtained values of peak force, perforation energy and flexural stiffness are very similar for the neat and the nanomodified joints. Furthermore, tests performed at different impact velocities showed that the effect of velocity is more evident when the peak force and the adsorbed energy are considered. Finally, the reduction of the flexural modulus after ten low energy impacts was significant but equivalent in the two joint types.

The introduction of nanoparticles in the tested thermoplastic adhesive is an interesting practice, because it allows for easier dismantling when required (for repairing or recycling) and it also has the potential to reduce the process time if suitable equipment is designed. Reversible adhesive nanomodified joints represent a valid and effective solution for assembling-disassembling structural components even when they are subjected to low-velocity impacts.

References

[1] Changa, B., Shi, Y., and Dong, S. J. Mater. Process. Technol. **87**,230–236 (1999).

[2] Belingardi, G., and Chiandussi G. Int. J. Adhes. Adhes. **24**,423-439 (2004).

[3] da Silva, L.F.M., Öchsner, A., and Adams, R.D. Handbook of Adhesion Technology (Springer Berlin Heidelberg, Berlin, 2011). 1st ed., Chap. 1, pp. 1-7.

[4] Machado, J.J.M., Marques, E.A.S., and da Silva, L.F.M. J. Adhes. 1-32 (2017).

[5] Pizzi, A., and Mittal, K. Handbook of Adhesive Technology (Marcel Dekker, Inc, New York, 2003). 2nd ed., Chap.1, pp. 10-21.

[6] Lutz, A. Structural bonding of lightweight cars – Report 299-52319-0515HMC, (The Dow chemical company. USA, Dow Automotive System, 2015).

[7] Mallik P., Materials, Design and Manufacturing for Lightweight Vehicles (Woodhead publishing, Dearborn, 2010). 1st ed., Chap. 10, pp. 384.

[8] Rudawska, A. Adhesive, application and properties (INTECH, Rijeka, 2016). 1st ed., Chap. 13, pp.341-362.

[9] Moritomi, S., Watanabe T., and Kanzaki S. Polypropylene Compounds for Automotive Applications – Report 2010-I. (Petrochemicals research laboratory. Japan, Sumitomo Kagaku, 2010).

[10] Ebnesajjad, S. Adhesives technology handbook (William Andrew Inc., Norwich, 2008) 2nd ed., Chap. 1, pp. 1-5.

[11] Nishimura, N., Simms, C.K., and Wood, D.P. Accid. Anal. Prev. **79**,1–12 (2015).

[12] Brach, R. "Modeling of Low-Speed, Front-to-Rear Vehicle Impacts" in SAE World Congress, Detroit, USA, 2003.

[13] Han., I. Proc. Inst. Mech. Eng. D J. Automob. Eng. **230**(4),554–563 (2016).

[14] Ciardiello, R., Belingardi, G., Martorana, B., Fondacaro, D., and Brunella, V. "A study of physical and mechanical properties of a nanomodified thermoplastic adhesive in normal and accelerated ageing conditions." in ECCM2016, Munich, Germany, 2016.

[15] Skeist, I. Handbook of adhesives. (Van Nostrand Reinhold, New York, 1990) 3rd ed. Chap. 43, pp. 705-712.

[16] Verna, E., Cannavaro, I., Brunella, V., Koricho, E.G., Belingardi, G., Roncato, D., Martorana, B., Lambertini, V., Neamtu, V.A., and Ciobanu, R. Int. J. Adhes. Adhes. **46**,21-25 (2013).

[17] Zinn, S., and Semiatin, S. Heat treat. Mag. 32-41 (1988).

[18] Koricho, E., Verna, E., Belingardi, G., Martorana, B., and Brunella, V. Int. J. Adhes. Adhes. **68**,164-181 (2016).

[19] Banea, M.D., da Silva, L.F.M., Campilho, R.D., and Sato, C. J. Adhes. **90**,16–40 (2014).

[20] Banea, M.D., da Silva, L.F.M., Carbas, R.C.J., and de Barros, S. J. Adhes. 1-15 (2016).

[21] Lin, J., Chang, L.C., Nien, M.H., and Ho, H.L. Compos. Struct. **74**,30–36 (2006).

[22] Avila, A.F., and Neto, A.S. Int. Mech. Eng. Congress. Expo. **15838**,643-650 (2006).

[23] Avila, A.F., Carvalho, M.G.R., Dias, E.C., and a Cruz, D.T.L. Compos. Struct. **92**,45–751 (2010).

[24] Xie, X., Li, R., Liu, Q., and Mai, Y. Polymer **45**,2793–2802 (2004).

[25] ASTM Standard E1876-09. (ASTM International, West Conshohocken, 2009).

[26] Belingardi, G., and Vadori, R. Compos. Struct. **61**,27–38 (2003).

[27] Belingardi, G., Cavatorta, M.P., and Paolino, D.S. ICCM, Proc. Int. Conf. Compos. Mater. **35**,609–619, 2008.

[28] Belingardi, G., Cavatorta, M.P., and Paolino, D.S. Compos. Sci. Technol. **69**,1693-1698. 2009.